

Torque driven ferromagnetic swimmers

Joshua K. Hamilton,^{a)} Andrew D. Gilbert, Peter. G. Petrov, and Feodor Y. Ogrin
College of Engineering, Mathematics and Physical Sciences, University of Exeter, Exeter EX4 4QF, UK

(Dated: 17 August 2018)

Microscopic swimming devices hold promise for radically new applications in lab-on-a-chip and microfluidic technology, including diagnostics and drug delivery. In this paper, we realize a macroscopic single particle ferromagnetic swimmer experimentally and investigate its swimming properties. The flagella-based swimmer is comprised of a hard ferromagnetic head attached to a flexible tail. We investigate the dynamic performance of the swimmer on the air-liquid interface as a function of the external magnetic field parameters (frequency and amplitude of an applied magnetic field). We show that the speed of the swimmer can be controlled by manipulating the strength and frequency of the external magnetic field (< 3.5 mT) and that the propagation direction has a dependence on parameters of the external magnetic field. The experimental results are compared to a theoretical model based on three beads, one of which having a fixed magnetic moment and the other two non-magnetic, connected via elastic filaments. The model shows sufficient complexity to satisfy the ‘non-reciprocity’ condition and gives good agreement with experiment. Via a simple conversion, we also demonstrate a fluid pump and investigate the induced flow. This investigation paves the way to the fabrication of such swimmers and fluid pump systems on a micro-scale, promising a variety of microfluidic applications.

I. INTRODUCTION

Externally controlled micro-robots have recently become an area of intense research because of their potential to contribute to a large range of applications. However, the experimental realization of such devices faces challenges due to the nature of their environments, namely propulsion at a low Reynolds number ($Re \ll 1$). The situation has been succinctly summarized by the so-called scallop theorem,^{1–3} stating a biological swimmer or any micro-scaled robot must have more than one degree of freedom to propel itself in a low Reynolds number environment.

In the past, many elegant models have been proposed showing methods of propulsion at low Reynolds numbers.^{4–9} Experimentally, the challenge remains in providing the micro device with significant energy and set of interactions to generate the required swimming motion. Thus, a range of different strategies have been proposed and employed, to varying levels of success, including ultrasound,¹⁰ electric,¹¹ and magnetic fields,^{12–19} as well as chemical reactions,^{20–24} and light driven systems.^{25,26}

As has been demonstrated in a number of cases, a typical approach to tackling the problem would be by mimicking the natural microscopic swimmers, such as sperm cells or bacteria. These systems would normally include magnetic beads for actuating and driving the swimmer in the liquid with an external magnetic field. The mechanism of motion in this case relies on the collective response of all particles. Even though the individual torques created on each bead is small the overall mechanics of the system is sufficient to generate a non-zero displacement.^{27,28}

Other approaches take advantage of the elastic properties of the tail, while applying the torque only to a single particle.^{29–37} For example, in a recent study by F. Box *et al.* a centimeter-scale system of elastically linked spheres was investigated, comprising of three spheres connected by unequal length elastic struts.³⁸ One of the spheres contained a fixed magnetic moment and the field was applied perpendicular to the moment. The propulsion mechanism was compared to the far-field description of a puller (a negative Stokes dipole).

Previously, we described theoretically and experimentally a highly efficient low Reynolds number swimmer based on the dipolar magnetic interaction between two magnetic particles of different anisotropy and size, elastically coupled together and actuated by an external magnetic field.^{39–44}

In this study, we discuss the properties and external responses of a self-propelled macro-scaled ferromagnetic swimmer based on only one magnetic particle. Experimentally this is implemented by using a high anisotropy magnetic bead - the head - attached to a flexible elastic filament - the tail - to mimic the structure of a beating flagellum. In order to describe this system, theoretically we use a simplified model based on multiple beads, in which the effect of the tail is represented by non-magnetic beads linked with massless elastic links. We show that even with the minimum of three particles (one magnetic and two non-magnetic, see Figure 1a) the system is able to self-propel and achieve the velocities comparable to those demonstrated experimentally.

In all cases the devices are activated and controlled by oscillating uniform magnetic field, in which the frequency and amplitude are varied to achieve different regimes of performance. A key variable which we have investigated is the effect of the tail length on the swimming performance. We also propose that such a swimmer can be converted into an efficient fluid pump.

^{a)}Corresponding author: jkh209@exeter.ac.uk

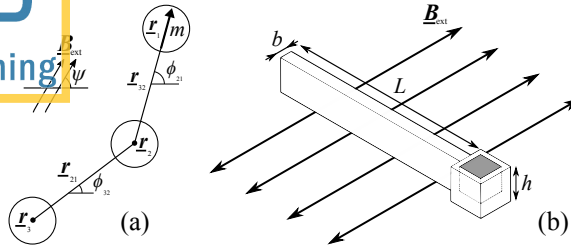


FIG. 1. (a) Geometrical configuration of the theoretical swimmer model, (b) schematic representation of the single ferromagnetic particle swimmer.

II. METHODOLOGY

The main feature of our experimental device is the magnetic 'head', which is made of a magnetically hard Nd-FeB cubic particle ($0.5 \text{ mm} \times 0.5 \text{ mm} \times 0.5 \text{ mm}$, Super Magnet Man, US). The NdFeB particle exhibits a high coercive field, due to its tetragonal crystal structure. The 'tails' were constructed using a 3D printed mold to produce the desired overall swimmer geometry (see Figure 1b). The mold was designed using Autodesk AutoCAD and 3D printed using a Formlabs Form 2, with clear resin (GPCL02) and cleaned by placing in isopropyl alcohol for 20 minutes. The magnetically hard ferromagnetic particle was fixed with its anisotropy axis along the tail axis of the swimmer, then the mold was filled with a Polycrat silicone rubber and fast cure catalyst (GP-3481-F) mixed with a weight ratio of 1:10 (catalyst:silicone). The length of the tails were varied in the range of $L = 1 - 12 \text{ mm}$, while keeping the head cubic ($h = 0.7 \text{ mm}$) and tail width ($b = 0.4 \text{ mm}$) constant. For all produced swimmers, the depth was kept at 0.7 mm, to ensure the complete encapsulation of the magnetic particle.

The swimming behavior of the macroscopic devices was studied by examining their mobility on a air-fluid interface of a large area Petri dish (148 mm diameter). The experimental setup comprised a Helmholtz coil system, powered with a sinusoidal signal, providing a uniform magnetic field to actuate and control the swimming devices. The frequency of the external field ranged between 30 and 170 Hz with magnetic fields up to 3.5 mT. The motion of the devices were observed using a video camera connected to a computer. Particle tracking software (Tracker⁴⁵) was used to determine the average speed and direction of propagation. A range of Reynolds numbers $\sim 3 \times 10^{-6} - 90$ have been investigated. The upper limit of the Reynolds number is due to a few factors, e.g. the high speeds which we observe at small tail lengths and the large characteristic length of the device at large tail lengths.

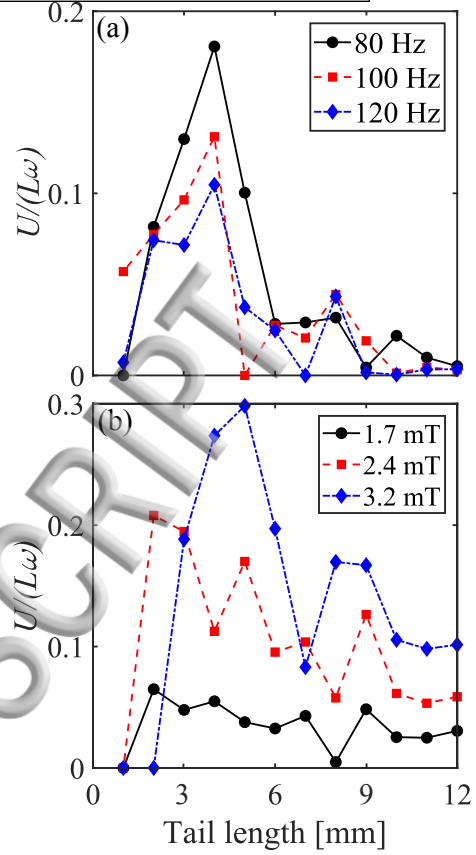


FIG. 2. dimensionless speed (by $L\omega$) as a function of tail length for (a) different frequencies - 80 Hz (black circle), 100 Hz (red square) and 120 Hz (blue diamond) - with an external magnetic field strength of 1.5 mT, (b) different magnetic field strengths - 1.7 mT (black circle), 2.4 mT (red square) and 3.2 mT (blue diamond) - with a fixed frequency of 50 Hz.

III. RESULTS AND DISCUSSION

A. Optimizing the single ferromagnetic particle swimmer

In previous investigations, the swimming behavior of flagella-like devices have been shown to have a dependence on the length of the flagellum, frequency of the applied field, the bending stiffness of the filament and the tail's fluid dynamic interactions.^{34,46} We investigated how external parameters of the magnetic field - frequency ω and field strength B - affect the swimmers, as well as tail length L . To find the optimum length of the swimmers tail, we created swimmers of different tail lengths and investigated the change in swimming performance for different field strengths and frequencies.

Figure 2a shows the range in performance of the swimming speed (scaled by $L\omega$) as a function of tail length for different frequencies. The magnetic field strength is fixed at 1.5 mT. There is a clear peak for all frequencies at $L = 4 \text{ mm}$. When the tail length is increased past the peak, the swimming speeds start to decrease for all fre-

quencies. We observe a maximum dimensionless speed of 0.18 corresponding to a real speed of 57.8 mm s^{-1} , with an external field of 1.5 mT and 80 Hz and a tail length of 4 mm.

Figure 2b shows a similar trend, but in this case for different field strengths, with a fixed frequency of 50 Hz. As the field strength is increased the overall speed of the swimming increases - due to the increased torque effects - as well as a peak at $L = 5 \text{ mm}$ manifesting at the higher field strengths. The maximum dimensionless speed in this case is 0.3 corresponding to a speed of 74.6 mm s^{-1} , with an external field of 3.2 mT and 50 Hz and a tail length of 5 mm.

Figure 2 shows that as the length of the tail becomes shorter ($L < 3 \text{ mm}$), the swimming performance begins to reduce; this is expected, due to the tail becoming effectively more rigid. For such conditions, the device becomes similar to a single degree of freedom reciprocal system and the scallop theorem will apply.¹ On the other hand, as the tail length is increased ($L > 10 \text{ mm}$), the elastic deformation or beating patterns become irregular, resulting in another reduction of swimming speed.

An important observation is that there is an obvious optimum length at which the swimming speed is maximized. This behavior can be linked to previous work,^{29,33} which shows a rapid decrease in swimming performance and irregular beading trajectories at large tail lengths. It also appears that there is also a second peak at $L = 8 \text{ mm}$ (Figure 2). It may be due to the second harmonic beating pattern, as the tail is twice the length of that for the first peak.

B. Directional control of the single ferromagnetic particle swimmer

Figure 3 shows a trajectory plot to visualize the direction of motion of the swimmer for different tail lengths and frequencies. The field direction is given in the last panel. We show the trajectories for four frequencies, 30 Hz (black circle), 80 Hz (red triangle), 130 Hz (blue square) and 170 Hz (green diamond). If the trace for a given frequency is not present, this is due to unstable propulsion of the swimmer for this combination of tail length and frequency.

Figure 3 clearly shows that as the frequency is increased for all tail lengths, the swimmer can be controlled for a range of propagation angles. The maximum angle of control $\sim 90^\circ$, can be observed in the $L = 12 \text{ mm}$ panel. The trajectories also visualize the variations of swimming speed with tail length, as the distance between the two points on the trajectories increases (the time between two points is kept constant at 0.2 seconds). For the swimmer with tail length less than 6 mm, the trajectories tend to be parallel to the applied magnetic field.

Typically, as the length of the tail is increased ($L > 6 \text{ mm}$), at low frequencies, the trajectories become perpendicular to the applied field. This mix of parallel and

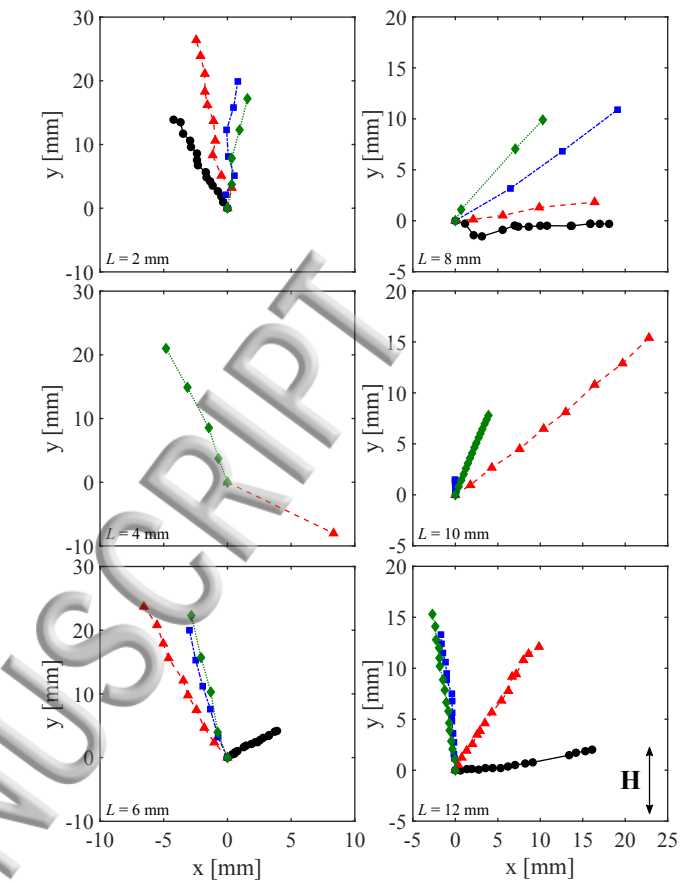


FIG. 3. Trajectory plots for tail lengths, 12 mm, 10 mm, 8 mm, 6 mm, 4 mm and 2 mm. The field has a strength of 1.5 mT and frequencies shown are 30 Hz (black circle), 80 Hz (red triangle), 130 Hz (blue square) and 170 Hz (green diamond). The swimmer is recorded for 20 seconds and the time between two points on a trajectory is 0.2 second.

perpendicular behavior is unexpected, one would expect the trajectories to be perpendicular to the applied field. [3 and 26] This could be due to irregular beating patterns created at large tail lengths, but could also be caused by additional degrees of freedom. These extra degrees of freedom could be caused in fabrication; there may be a small out-of-plane magnetic component, resulting in a rocking in the z-plane when the external field is applied. As the devices are placed on the surface of the fluid, this could also cause extra asymmetries in the motion, due to boundary effects. At the air-liquid interface, the force arising from the surface tension confines the swimmer to the liquid surface as it acts against swimmers motion in the z-direction (i.e. in the direction normal to the liquid surface). This behavior could also be explained by the increased Reynolds number for the larger values of L , resulting in inertia effects being present.

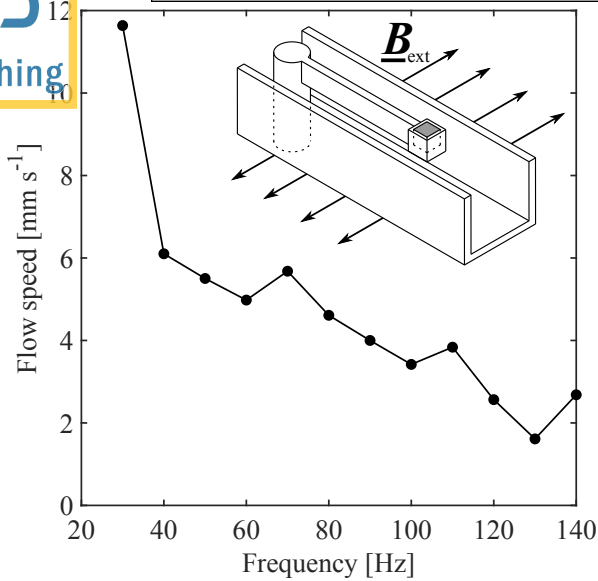


FIG. 4. Swimming speed as a function of dynamic viscosity. The solid red line indicates the predicted values from the theory (equation 10). The external magnetic field has strength 3.0 mT and frequency 50 Hz. The Reynolds numbers shown here are: 90 (for $\eta = 1 \times 10^{-3}$ Pa s), 0.53 (for $\eta = 1 \times 10^{-2}$ Pa s), 1.6×10^{-4} (for $\eta = 0.1$ Pa s) and 2.5×10^{-6} (for $\eta = 1$ Pa s).

C. Viscosity dependency of the single ferromagnetic particle swimmer

Figure 4 shows the swimming speed of a single particle swimmer with $L = 3$ mm for fluids of different viscosities. The dynamic viscosity ranges from 1×10^{-3} Pa s (100% water) to 1.4 Pa s (100% glycerol). The external magnetic field has a frequency of 50 Hz and strength of 3.0 mT. The predicted velocities are shown with the solid red line - using the experimental parameters with no fitted parameters and equation 10 (see below). The experiment and theory show good agreement, except for the most viscous data where the experiment is out performing the theoretical prediction. The differences between the theory and experiment may arise from the simplifications made in the theory. Figure 4 shows that the swimmer can successfully propel at both low and moderate Reynolds number - given the Reynolds number range of $\sim 3 \times 10^{-6} - 90$.

D. Fluid pumping with the single ferromagnetic particle swimmer

A swimming device can easily be converted into a pumping device by a change of reference frame. This can be done by restricting the translational motion of the swimmer when actuated. In the case of the single ferromagnetic particle swimmer, it is possible to attach one end to the top of an elastic pin (Figure 5 inset). Instead of pro-

pelling itself through the fluid, the swimmer now induces a fluid flow.

In this configuration, the pinned swimmer rests gently on the surface of the fluid (supported by surface tension forces) and the fluid flow it generates can conveniently be investigated. As an example of this application we attach the pinned swimmer (tail length of 7 mm) within a 3D printed straight channel with width of 5 mm and depth of 10 mm. The flow speed is determined by placing small (~ 0.2 mm) particles of graphite on the air-fluid interface and following them using the previous tracking software. In this investigation, we apply the external magnetic field perpendicular to the channel.

Figure 5 shows the frequency dependence of the induced flow speeds driven by an actuating magnetic field of 1.5 mT. The figure shows a maximum in flow speed at 30 Hz, then over 40 - 140 Hz a gradual decrease in flow speed between 6 mm s^{-1} and 2 mm s^{-1} . We can define the effectiveness (χ) of the system as the ratio between the real speed range of a free swimmer and the induced flow speed. If we investigate the stable range of the system 40 - 140 Hz, we find $\chi_{7\text{mm}} = 0.31 \pm 0.07$, where the uncertainty is half a standard deviation. This system shows a stable flow speed over the operating regime of the device. A possible way to improve the effectiveness would be to restrict the translational motion with less effects on the beating pattern. The only concern with such a system is that as the channel width is reduced, the pump could obstruct too much of the channel and the viscous friction will be increases, this may result in a reduced flow rate. The concern could be addressed by scaling the pump with the channel, or incorporating the system into the walls of the channel.

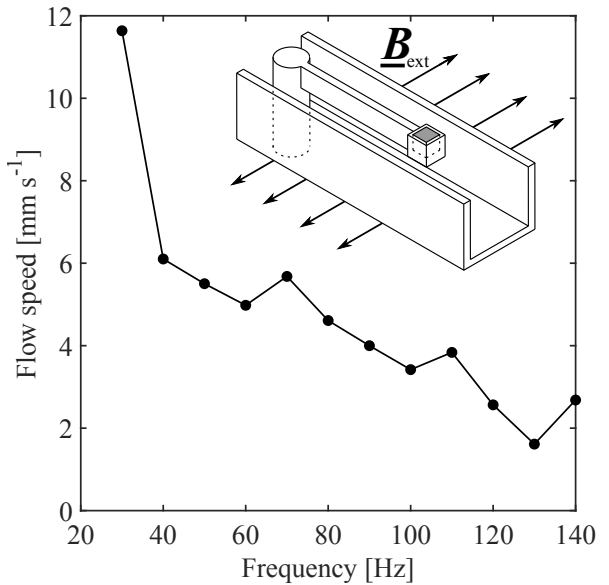


FIG. 5. Measured flow speed along the channel as a function of frequency. The inset shows a schematic representation of the single ferromagnetic particle swimmer as a fluid pump. The base of the pin is attached to the base of the channel.

THREE PARTICLE THEORETICAL MODEL

To elucidate the swimmer mechanism, we have developed a minimal theoretical model in which three spherical particles labeled by $j = 1, 2, 3$, are connected via elastic filaments, as depicted in Figure 1a. The particles have radii R_j and are centered at $\mathbf{r}_j(t) = (x_j(t), y_j(t))$; the center of reaction⁴⁷ is $\mathbf{X} = (X, Y)$ given by

$$\mathbf{X} \sum_j R_j = \sum_j R_j \mathbf{r}_j.$$

We set $\mathbf{r}_{jk} = \mathbf{r}_k - \mathbf{r}_j$, $r_{jk} = |\mathbf{r}_{jk}|$, $\hat{\mathbf{r}}_{jk} = r_{jk}^{-1} \mathbf{r}_{jk}$, and let ϕ_{jk} be the angle \mathbf{r}_{jk} makes with the x -axis. Particle motion is governed by

$$\mu_j \ddot{\mathbf{r}}_j = \mathbf{F}_{\text{spring},j} + \mathbf{F}_{\text{bend},j} + \mathbf{F}_{\text{ext},j} + \mathbf{F}_{\text{fluid},j}, \quad (1)$$

with masses μ_j taken to be sufficiently small that the motion is in an inertia-free Stokes regime (the results are insensitive to the values of μ_j in the limit $\mu_j \rightarrow 0$). The following forces are derived from potentials, first elastic forces

$$V_{\text{spring}} = \frac{1}{2} k(r_{21} - l_0)^2 + \frac{1}{2} k(r_{32} - l_0)^2,$$

where l_0 is each filament's natural length and k is a spring constant. Second, we impose a force resisting bending motion of the three particle configuration, derived from the potential

$$V_{\text{bend}} = -\ell \cos(\phi_{21} - \phi_{32}).$$

Since $\cos \varepsilon = 1 - \varepsilon^2/2 + \dots$, this is quadratic for small angle, but being periodic in the angle does not result in numerical problems if an angle jumps by 2π in our simulations.

The external magnetic field \mathbf{B}_{ext} drives the swimmer directly through a potential term, on magnet $j = 1$,

$$V_{\text{ext}} = -\mathbf{m} \cdot \mathbf{B}_{\text{ext}} = -m B_{\text{ext}} b(t) \cos(\phi_{21} - \psi(t)),$$

where the field has magnitude $B_{\text{ext}} b(t)$ and angle $\psi(t)$ to the x -axis. Here B_{ext} is a constant and $b(t)$ and $\psi(t)$ are dimensionless. The field is taken to be purely back-and-forth along the y -axis,

$$\mathbf{B}_{\text{ext}} = B_{\text{ext}}(0, \sin \omega t). \quad (2)$$

Provided the radii $R_j \ll l_0$, the length of the connecting filaments, we may write the force on each bead from the surrounding fluid as expansions that include Stokes drag and the leading order fluid interaction term^{47,48},

$$\begin{aligned} \mathbf{F}_{\text{fluid},j} &= \mathbf{F}_{\text{drag},j} + \mathbf{F}_{\text{interact},j} \\ &= -6\pi\eta R_j \dot{\mathbf{r}}_j + \sum_k \frac{9\pi}{2} \frac{\eta R_j R_k}{r_{jk}} (\hat{\mathbf{r}}_{jk} \hat{\mathbf{r}}_{jk} + I) \cdot \dot{\mathbf{r}}_k, \end{aligned} \quad (3)$$

where I is the identity matrix. Here and below we exclude the term when $j = k$ without comment. These are

the leading terms in an expansion in the small parameter $\varepsilon = R/l_0 \ll 1$ where $R = \frac{1}{3}(R_1 + R_2 + R_3)$ is the average bead radius, say. At this level of approximation the motion of the center of reaction is given by

$$\begin{aligned} 6\pi\eta \left(\sum_j R_j \right) \dot{\mathbf{X}} &= \sum_j \mathbf{F}_{\text{interact},j} \\ &= \sum_{j,k} \frac{9\pi}{2} \frac{\eta R_j R_k}{r_{jk}} (\hat{\mathbf{r}}_{jk} \hat{\mathbf{r}}_{jk} + I) \cdot \dot{\mathbf{r}}_k. \end{aligned} \quad (4)$$

The parameters introduced are $\{\mu_j, R_j, k, l_0, \ell, m, B_{\text{ext}}, \omega, \eta\}$ and it is convenient to define length, time and mass scales via

$$l_0 = \mathcal{L}, \quad \omega^{-1} = \mathcal{T}, \quad \ell l_0^{-2} \omega^{-2} = \mathcal{M},$$

and key dimensionless parameters⁴⁰

$$\begin{aligned} \varepsilon &= \frac{R}{\mathcal{L}}, \quad \varpi = \varepsilon \frac{\mathcal{L}\mathcal{T}}{\mathcal{M}} 6\pi\eta = \frac{\omega l_0^2 R}{\ell} 6\pi\eta, \\ A_{\text{ext}} &= m B_{\text{ext}} \frac{\mathcal{T}^2}{\mathcal{M}\mathcal{L}^2} = \frac{m B_{\text{ext}}}{\ell}. \end{aligned}$$

Note that the quantity A_{ext} is sometimes called the magnetoelastic number, and ϖ is closely linked to the ratio of swimmer length to the elastic penetration length, e.g. in R. Livanovičs *et al.*³² We use the following experimental parameter values for simulations,

$$\begin{aligned} R &= 1.25 \times 10^{-3} \text{ m}, \quad k = 1.67 \times 10^{-2} \text{ N m}^{-1}, \\ l_0 &= 5 \times 10^{-3} \text{ m}, \quad \ell = k l_0^2 = 4.2 \times 10^{-7} \text{ J}, \\ m &= 1.2 \times 10^{-4} \text{ A m}^2, \quad B_{\text{ext}} = 3 \times 10^{-3} \text{ T}, \\ \omega &= 100 \times 2\pi \text{ s}^{-1}, \quad \eta = 10^{-3} \text{ Pa s}, \end{aligned}$$

yielding

$$\begin{aligned} \mathcal{L} &= 5 \times 10^{-3} \text{ m}, \quad \mathcal{T} = 1.6 \times 10^{-3} \text{ s}, \quad \mathcal{M} = 4.2 \times 10^{-8} \text{ kg}, \\ \varepsilon &= 0.25, \quad \varpi = 0.89, \quad A_{\text{ext}} = 0.86, \end{aligned}$$

but should note that our idealized model is only expected to allow qualitative comparison with the experiments. The theory developed below gives an approximation to the swimming speed as

$$\dot{\mathbf{X}} = \varepsilon l_0 \omega \frac{21 A_{\text{ext}}^2}{16 \varpi (\varpi^2 + 36)} \simeq 2.4 \times 10^{-2} \text{ m s}^{-1}. \quad (5)$$

The value for the swimming speed shown in equation (5) can be compared with the typical value of speed shown experimentally. Comparing to the experimental data, the velocities range $\sim 5 \text{ mm s}^{-1} - 70 \text{ mm s}^{-1}$. This comparison gives good order of magnitude agreement and provides support for the model, despite its idealized nature - simplified geometry and elastic properties.

Differences between the model could also arise from the swimmer being modeled within the bulk of the fluid. In the experiment the swimmer is mainly confined to the interface, with only part of the body submerged into the

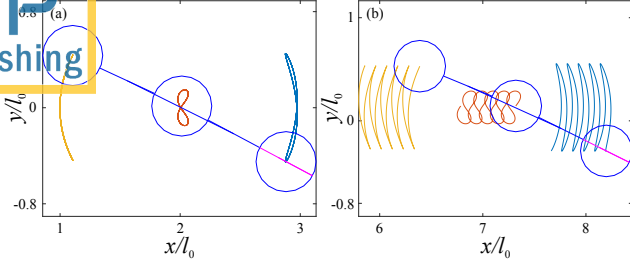


FIG. 6. (a) The motion of the swimmer without fluid interactions, to visualize how time-reversibility is broken. (b) The overall motion of the modeled swimmer with fluid interactions.

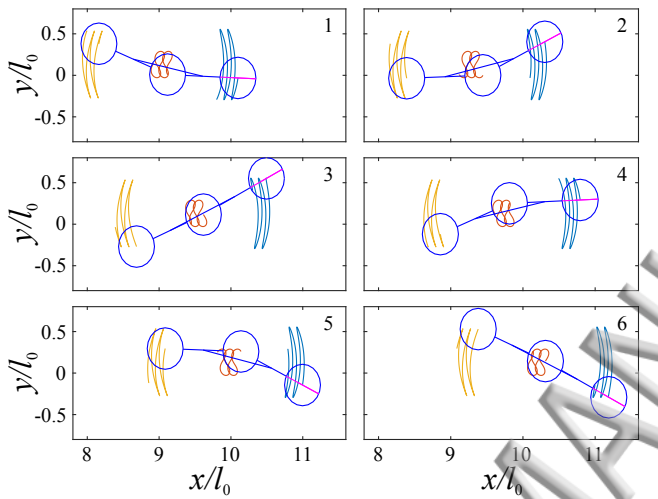


FIG. 7. A series of snap-shots showing the motion of the modeled three-particle swimmer, with each panel separated by $2\frac{1}{6}$ cycles of the external field. The sequence reads left to right.

liquid. With contact angle being close to 90 degrees, the translational motion of the swimmer is still governed by the same principles as those in the model.

Figure 6a shows the motion of the swimmer using the above parameter values with no fluid interactions between particles. The figure of eight motion of each particle, observed in one full cycle, shows how the swimmer breaks time-reversibility, while the center of reaction remains fixed. Once the fluid interactions are turned on in the simulation, the swimmer now propels itself through the fluid (Figure 6b), as seen in a series of snap-shots in Figure 7.

Figure 8 shows the frequency dependence of the swimming speed when A_{ext} takes the above value (top solid curve in red) and when it is reduced to 80%, 60%, etc (other solid curves). For all values of A_{ext} the simulated velocities show a peak for low frequencies ($\varpi < 1$). This can be compared to the suppression of the maximum in experimental speed shown in Figure 2, as the frequency is increased - and fixed tail length. The agreement be-

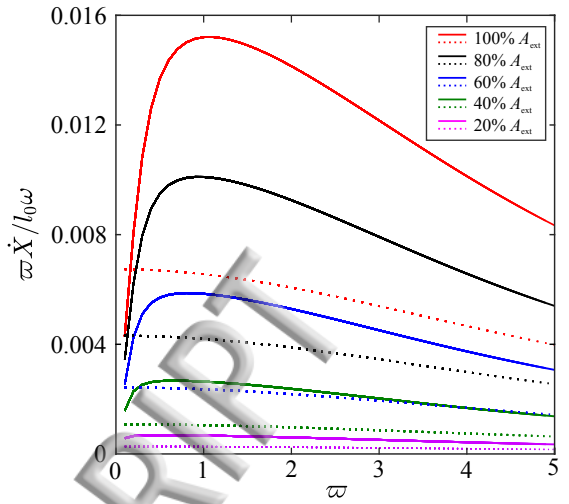


FIG. 8. Scaled non-dimensional speed as a function of frequency for different values of A_{ext} . The solid line indicates the simulation, the dotted indicates the theory.

tween simulated swimming velocities (solid curves) and the theory - shown later - (dotted curves) is not particularly good; we note however that the theory is based on linearized internal motion and on weak fluid interactions, requiring that A_{ext} and ε are both small and ϖ is of order unity. Further simulations (not reported here) confirm that the theory does in fact becomes accurate in the limit of small A_{ext} and ε with $\varpi = O(1)$. While it cannot be used for quantitative information at these parameter values, we argue that it does capture the underlying mechanism and give correct order-of-magnitude estimates; a more accurate theory would require a computational fluid dynamics (CFD) approach. Note that for clarity we have plotted the quantity $\varpi \dot{X}/l_0 \omega$ for which the frequency ω of the field is scaled out (by virtue of the definition of ϖ). Thus this figure gives a quantity proportional to the observed swimming speed in the laboratory (that is, not divided by the field frequency).

Figure 9 shows the frequency dependence of the swimming speed for different numbers of linked particles. The investigation ranges from the standard $n = 3$ particle system increasing to $n = 8$, with ε now reduced to $\varepsilon = 0.1$. Note that in our formulation the total swimmer length is $(n - 1)l_0$ and we have scaled the swimming speed by l_0 not by the total length. For all particle systems a peak in swimming performance is observed.

Two noteworthy observations are that for low frequency ($\varpi < 1$) the propulsion speed is lowest for the 3 particle system, then increases to a peak at the 4 particle system, then decreases with increasing numbers of particles (Figure 9). We also note that for large frequencies ($\varpi > 2$) the propulsion speed is highest for the 3 particle system and decreases with increasing number of particles.

Figure 10 shows the dependency of the number of

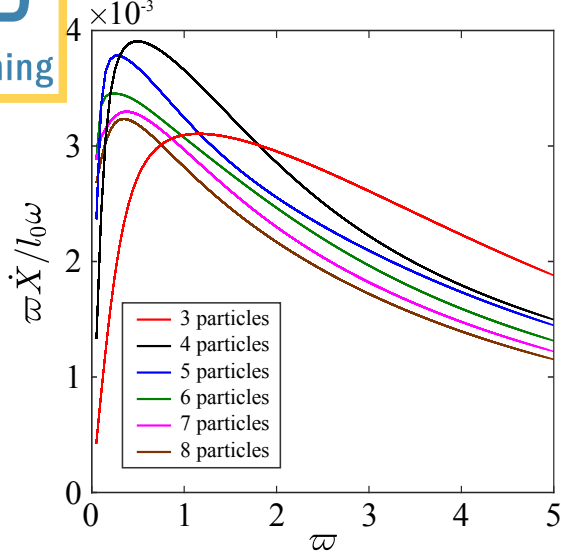


FIG. 9. Scaled non-dimensional speed as a function of frequency for different numbers of linked particles, with $\varepsilon = 0.1$.

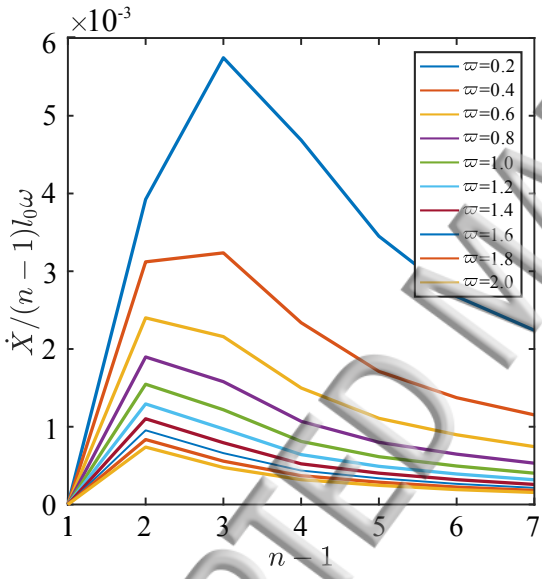


FIG. 10. Scaled non-dimensional speed as a function of number of linked particles for different frequencies, with $\varepsilon = 0.1$.

linked particles on the swimming speed. The investigation ranges from $n = 2$ to $n = 8$, for different values of the frequency. For all cases, we observe a rise to a peak ($\approx n = 3$) then a steady decrease in speed. This is in agreement with results for flexible-tailed swimmers, Figure 7 of R. Livanovićs *et al.*,³² which shows similar peaks in velocity as a function of swimmer length. As the frequency increases, the peak speed is reduced - similar to that seen in the experiment (Figure 2). For frequencies where $\bar{\omega} \leq 0.4$ we observe a peak at $n = 4$, as the frequencies increases ($\bar{\omega} \geq 0.6$), the maximum shifts towards $n = 3$.

We now give the theory leading to (5). In our approximate model we start with the swimmer beads located at $(l_0, 0)$, $(0, 0)$ and $(-l_0, 0)$ for $j = 1, 2, 3$, respectively and linearize the equations of motion for small displacements, neglecting any fluid interaction forces. We take the driving magnetic field to be given in (2), zero inertia $\mu_j = 0$ and beads of equal radius $R_j = R$ for simplicity; the framework is easily generalized to any number of beads and any radii. The linearized equations only involve the transverse displacements y_j and take the form

$$6\pi\eta R \dot{\mathbf{y}} = \ell l_0^{-2} M \mathbf{y} + m B_{\text{ext}} l_0^{-1} \sin \omega t \mathbf{w},$$

$$M = \begin{pmatrix} -1 & 2 & -1 \\ 2 & -4 & 2 \\ -1 & 2 & -1 \end{pmatrix}, \quad \mathbf{w} = \begin{pmatrix} 1 \\ -1 \\ 0 \end{pmatrix}, \quad \mathbf{y} = \begin{pmatrix} y_1 \\ y_2 \\ y_3 \end{pmatrix}.$$

We now extract a harmonic by setting $\mathbf{y} = l_0 \hat{\mathbf{y}} e^{i\omega t} + \text{c.c.}$. The factor l_0 makes the vector $\hat{\mathbf{y}}$ dimensionless and the governing equations then become

$$i\bar{\omega} \hat{\mathbf{y}} = M \hat{\mathbf{y}} - \frac{1}{2} i A_{\text{ext}} \mathbf{w} \quad (6)$$

This can be inverted to give $\hat{\mathbf{y}}$ and the *internal motion* of the swimmer reconstructed, in other words giving the balance between elastic forces, Stokes drag and magnetic driving, but excluding fluid interactions in (3)

The actual swimming speed is then given at leading order by substituting the internal motion into the equation (4) for the center of reaction. At leading order in perturbation theory this is given by quadratic terms and the average speed in the x -direction is then

$$\dot{X} = \frac{1}{4} R l_0^{-2} \langle \mathbf{y}^T N \hat{\mathbf{y}} \rangle, \quad N = \begin{pmatrix} 0 & 1 & \frac{1}{4} \\ -1 & 0 & 1 \\ -\frac{1}{4} & -1 & 0 \end{pmatrix}, \quad (7)$$

where the angled brackets denote a time average. This becomes

$$\dot{X} = \frac{1}{2} i \varepsilon l_0 \omega \hat{\mathbf{y}}^{*T} N \hat{\mathbf{y}}, \quad (8)$$

noting that $l_0 \omega = \mathcal{L}/\mathcal{T}$ are the units of speed in our non-dimensionalisation, that is, motion of the swimmer is measured in units of link length per cycle, multiplied by ε reflecting the fact that it is the weak fluid interactions that are key to motion of the center of reaction.

Although a similar system is easily written down for any number of beads, the advantage of dealing with just three is that the problem may be solved analytically. The matrix M has eigenvectors $\mathbf{v}_1 = (1, 1, 1)^T$ eigenvalue $\lambda_1 = 0$ (a translation mode), $\mathbf{v}_2 = (1, 0, -1)^T$, $\lambda_2 = 0$ (a rotation mode) and $\mathbf{v}_3 = (1, -2, 1)^T$, $\lambda_3 = -6$ (a bending mode). The magnetic driving excites the latter two since $\mathbf{w} = \frac{1}{2}\mathbf{v}_2 + \frac{1}{2}\mathbf{v}_3$ and then we can express the solution to (6) as

$$\hat{\mathbf{y}} = -\frac{1}{4} A_{\text{ext}} [\bar{\omega}^{-1} \mathbf{v}_2 + (\bar{\omega} - 6i)^{-1} \mathbf{v}_3] \quad (9)$$

We drive two modes and this is crucial for swimming. Now $\mathbf{v}_2^T N \mathbf{v}_3 = -\mathbf{v}_3^T N \mathbf{v}_2 = -7/2$ and thus after a short

calculation we obtain the swimmer speed from (8) as

$$\frac{\dot{X}}{l_0\omega} = \varepsilon \frac{21A_{\text{ext}}^2}{16\varpi(\varpi^2 + 36)}. \quad (10)$$

The velocity here is normalized in terms of body length per (radian of the) magnetic field cycle. The right-hand side diverges as $\varpi \rightarrow 0$, which is unphysical, but in reality the linearization would break down in this limit and the model is not applicable.

Note that we need to drive two distinct modes to ‘break’ the scallop theorem and that the translation mode v_1 cannot be excited externally as there is no net force on the swimmer; thus the three-particle swimmer here is a minimal model. For a three-particle model of a biological swimmer (without any external torques or forces), the second mode v_2 also could not be generated and only v_3 could be, leading to precisely a scallop type motion and no swimming. A key point is that the external field provides torques on the swimmer and allows a three-particle swimmer to work. A four-particle model would allow for a biological swimmer; translation and rotation modes could not be excited, but this would still leave two bending modes which could be employed to give non-reversible internal motion and so swimming. Although these remarks are for idealized multi-bead swimmers, they are relevant to more realistic geometry, here with a head and elastic tail,^{33,38} when the finite set of bending modes discussed above would be replaced by the leading bending modes from an infinite set.

V. CONCLUSIONS

In summary, we present a macroscopic investigation of a single ferromagnetic particle swimming device based on the bending of a flexible tail. The device was actuated and controlled by an oscillating magnetic field (< 3.5 mT). This investigation involved the fabrication of the device and its characterization by device and external parameters (tail length, field strength and frequency). The frequency and tail length response showed that there is an optimum tail length of 4 mm, corresponding to speed of propulsion and control of direction.

The single ferromagnetic particle swimmer was shown to successfully propel at a range of Reynolds numbers $\sim 3 \times 10^{-6} - 90$.

This investigation of macroscopic scaled swimmers, helps understand the swimming behavior of artificial flagella-based swimmers, and paves the way for fabricating optimum microscopic magnetic flagella-based swimmers.

We also present a theoretical model comprising of three particles, one of which is magnetic, to describe the basic motion of the swimmer in the low Reynolds number regime. We show that there are three main modes of the system. However, we only excite the two modes (rotation and bending) that are crucial for swimming at a

low Reynolds number. There is no external force so the translational mode is not excited. The model shows a quantitative agreement with experiment, even with its simplified geometry and elastic properties.

In addition to the investigation of the free swimmer, we also present a way to use such a device as a fluid pump. The system was shown to induce a flow which was stable over the operating range of the device, with an effectiveness $\chi_{7\text{mm}} = 0.31 \pm 0.07$. Such a system holds promise to be used as a microfluidic pump embedded into a lab-on-a-chip system for microfluidic manipulation.

SUPPLEMENTARY MATERIAL

See supplementary material for real time videos showing the translational motion of the single ferromagnetic particle swimmer.

ACKNOWLEDGEMENTS

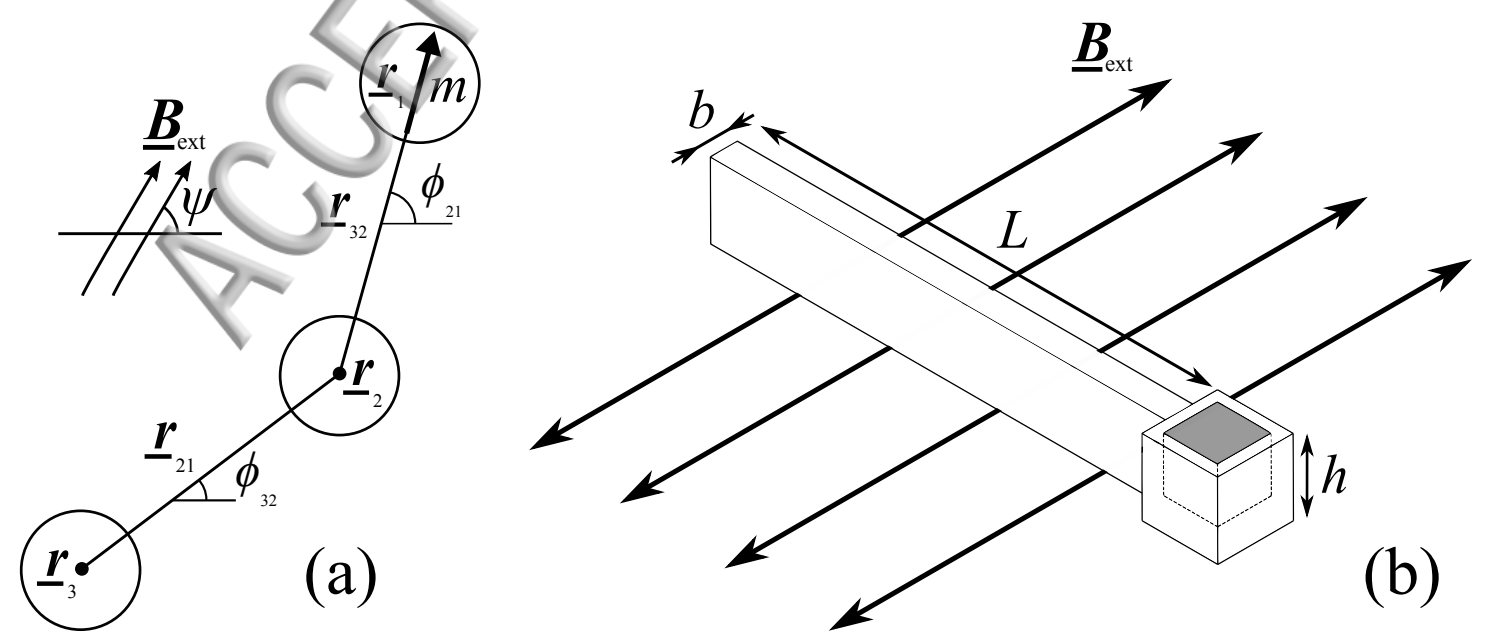
This project has received funding from the European Unions Horizon 2020 research and innovation programme under grant agreement No. 665440. We also acknowledge support via the EPSRC Centre for Doctoral Training in Metamaterials (Grant No. EP/L015331/1).

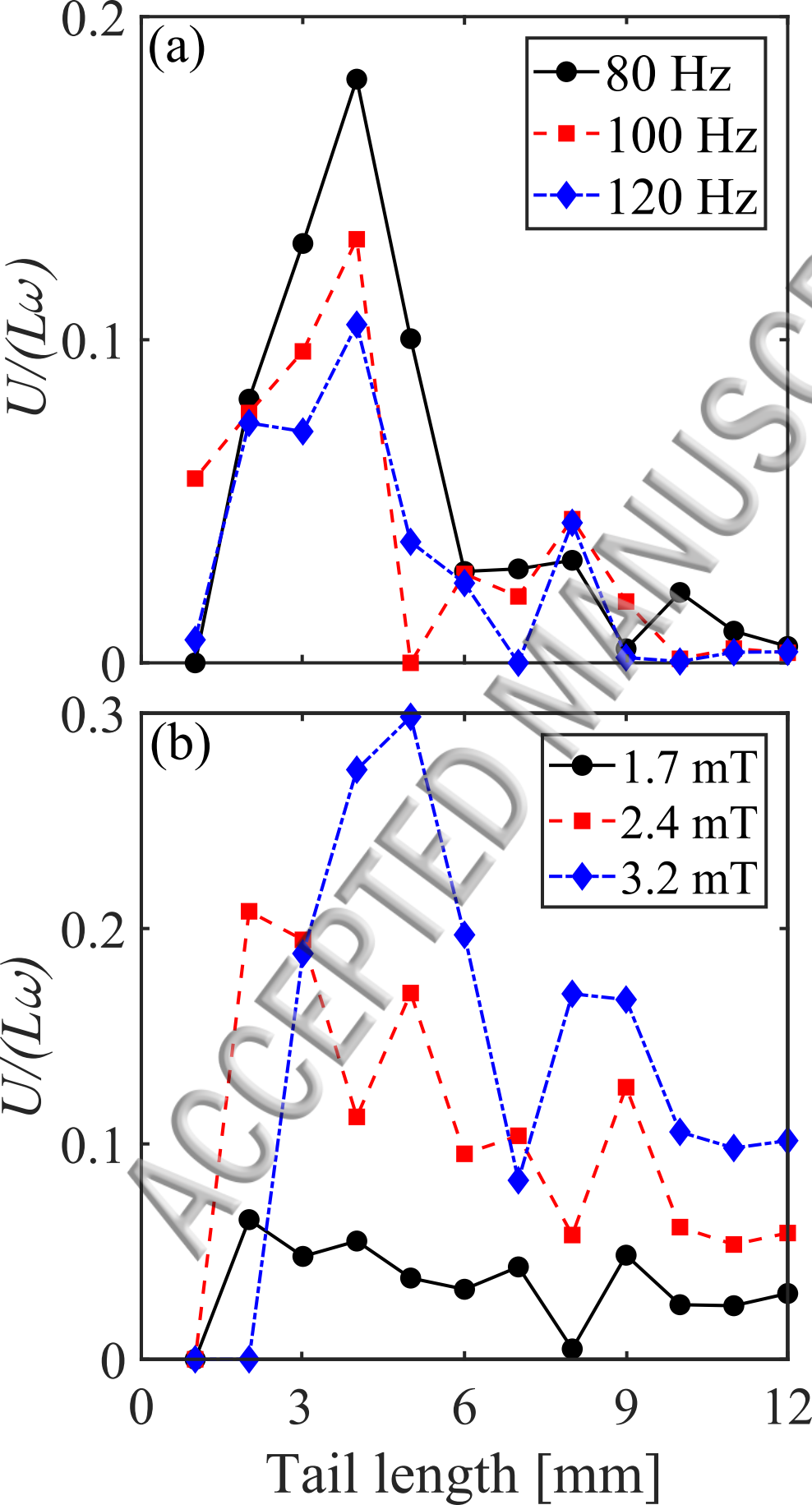
REFERENCES

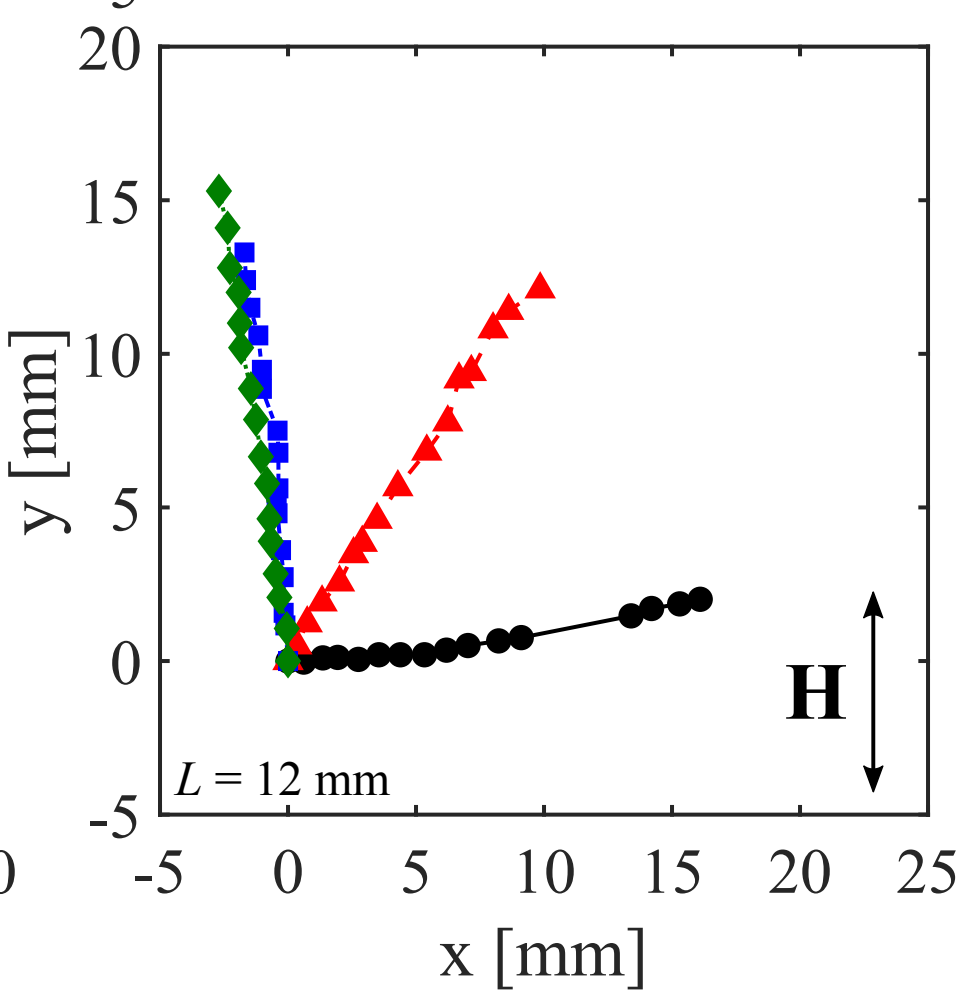
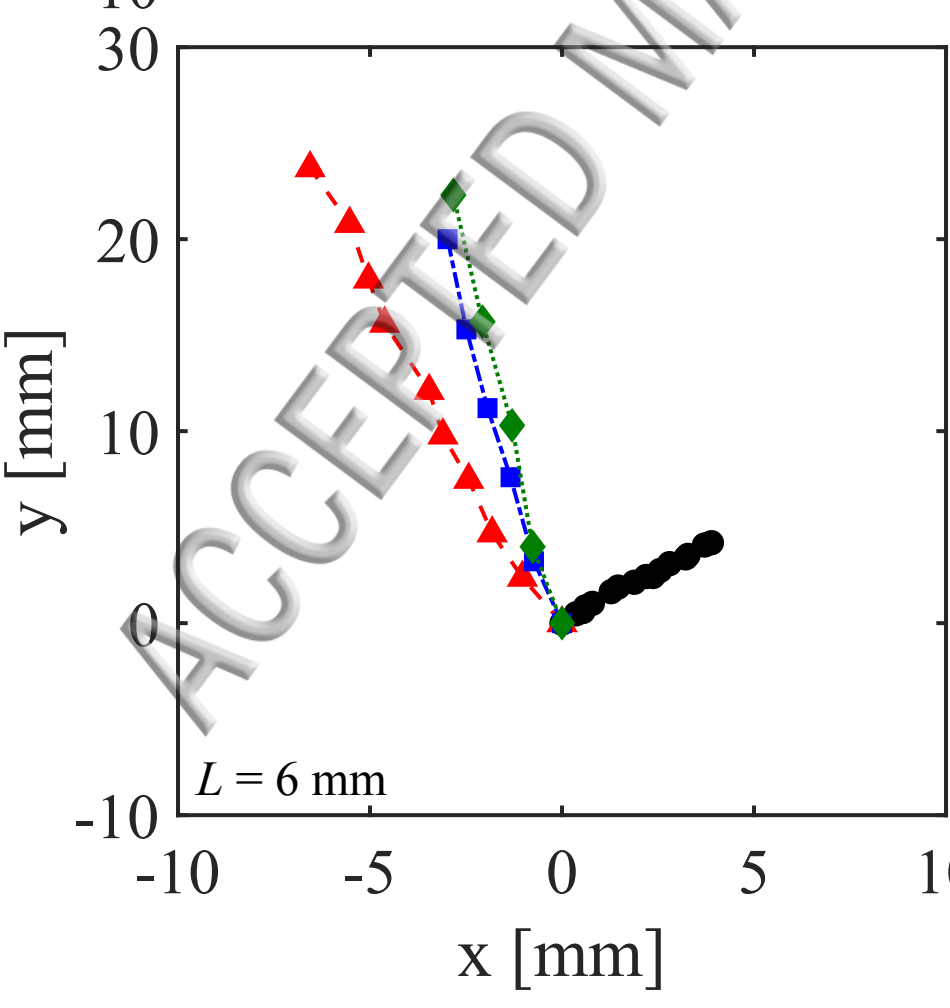
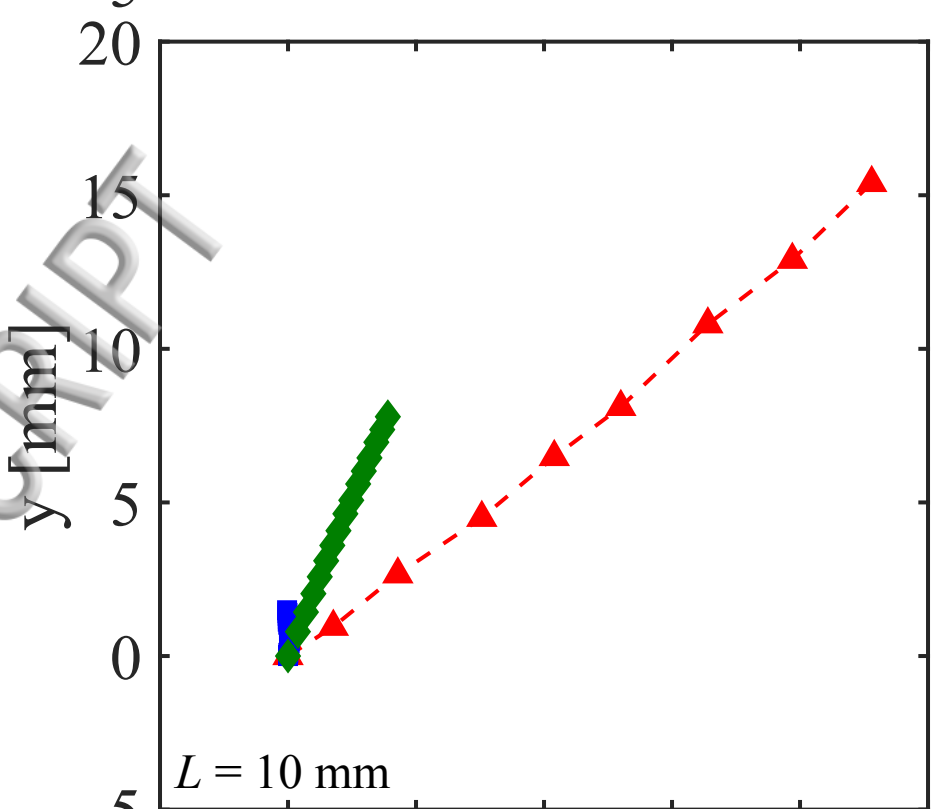
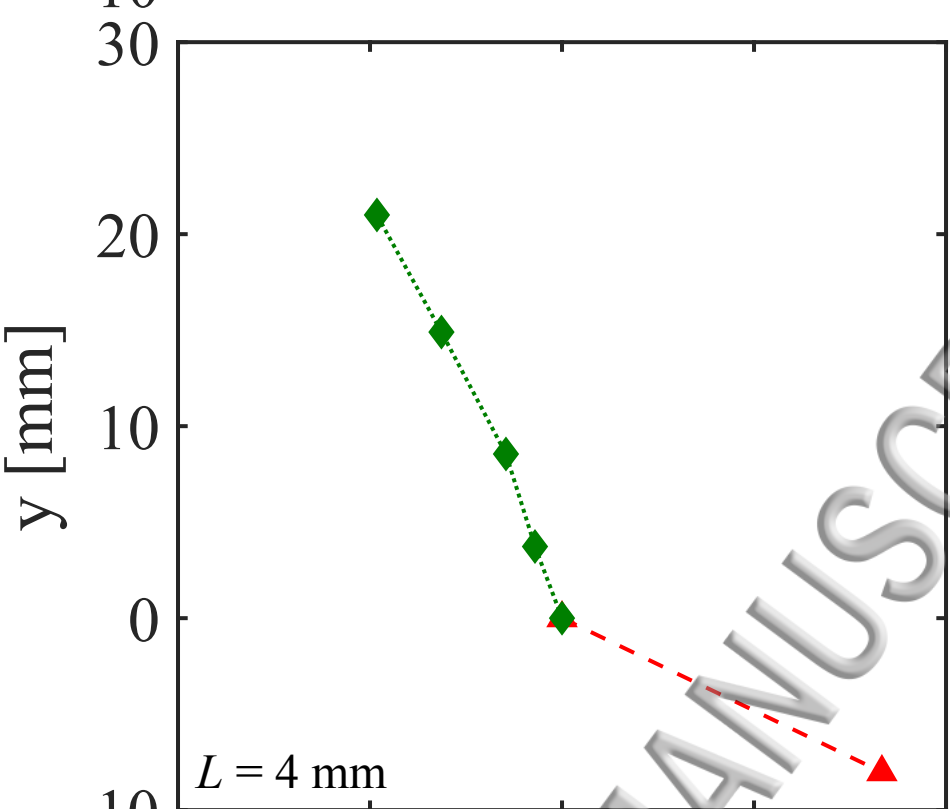
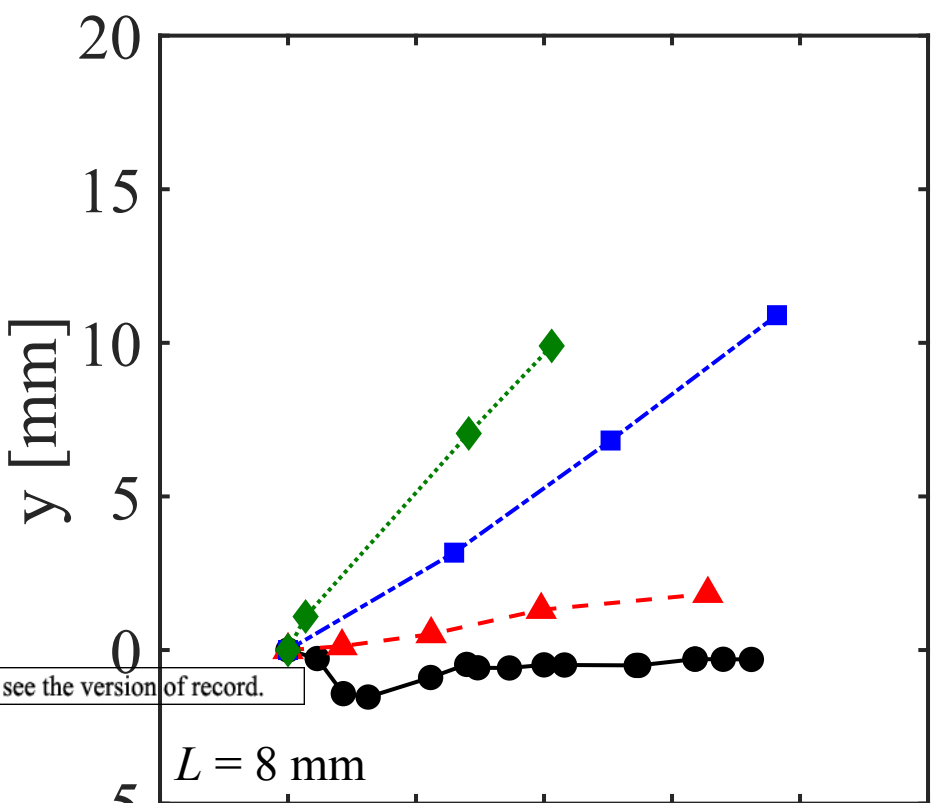
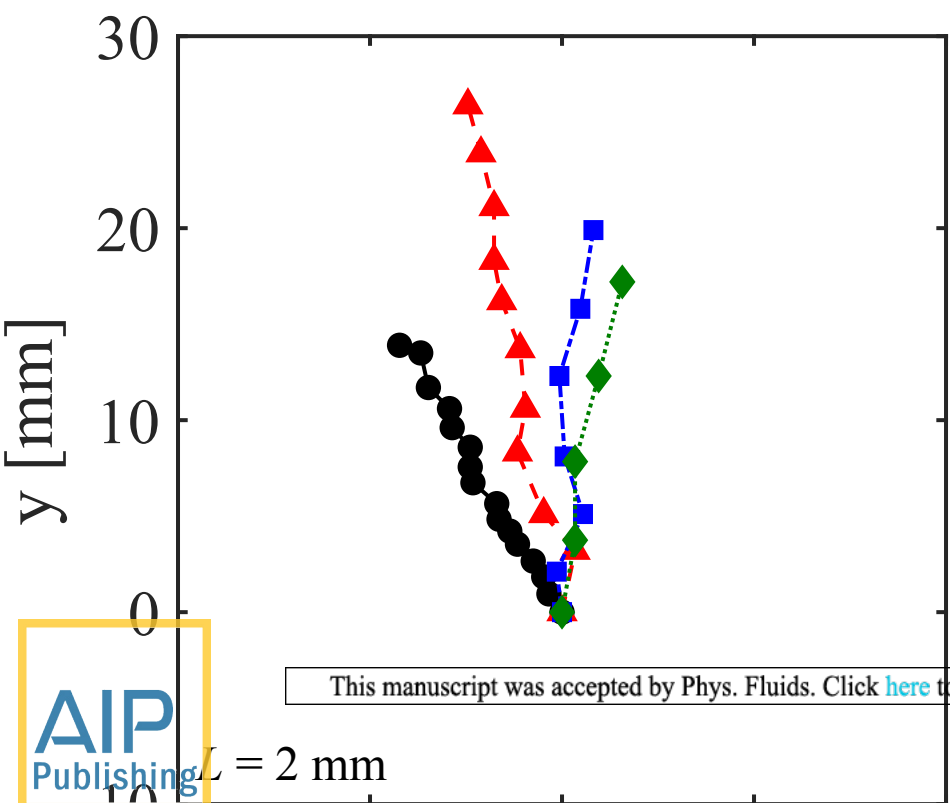
- ¹E. M. Purcell, American Journal of Physics **45**, 3 (1977).
- ²A. Shapere and F. Wilczek, Journal of Fluid Mechanics **198**, 557 (1989).
- ³E. Lauga and T. R. Powers, Reports on Progress in Physics **72**, 096601 (2009).
- ⁴A. Najafi and R. Golestanian, Physical Review E - Statistical, Nonlinear, and Soft Matter Physics **69** (2004).
- ⁵A. Najafi and R. Zargar, Physical Review E - Statistical, Nonlinear, and Soft Matter Physics **81**, 1 (2010).
- ⁶M. Leoni, B. Bassetti, J. Kotar, P. Cicuta, and M. Cosentino Lagomarsino, Physical Review E - Statistical, Nonlinear, and Soft Matter Physics **81**, 1 (2010).
- ⁷D. Salazar, A. M. Roma, and H. D. Ceniceros, Physics of Fluids **28** (2016).
- ⁸E. J. Campbell and P. Bagchi, Physics of Fluids **29**, 101902 (2017).
- ⁹S. Yazdi and A. Borhan, Physics of Fluids **29** (2017).
- ¹⁰K. J. Rao, F. Li, L. Meng, H. Zheng, F. Cai, and W. Wang, Small **11**, 2836 (2015).
- ¹¹S. T. Chang, V. N. Paunov, D. N. Petsev, and O. D. Velev, Nature materials **6**, 235 (2007).
- ¹²K. Ishiyama, M. Sendoh, A. Yamazaki, and K. I. Arai, Sensors and Actuators, A: Physical **91**, 141 (2001).
- ¹³P. Tierno, R. Golestanian, I. Pagonabarraga, and F. Sagués, Journal of Physical Chemistry B **112**, 16525 (2008).
- ¹⁴S. Tottori, L. Zhang, F. Qiu, K. K. Krawczyk, A. Franco-Obregón, and B. J. Nelson, Advanced Materials **24**, 811 (2012).
- ¹⁵M. Medina-Sánchez, L. Schwarz, A. K. Meyer, F. Hebenstreit, and O. G. Schmidt, Nano letters **16**, 555 (2015).
- ¹⁶G. Grosjean, G. Lagubeau, A. Darras, M. Hubert, G. Lumay, and N. Vandewalle, Nature communications **1**, 1 (2015).

- ¹⁷A. M. Maier, C. Weig, P. Oswald, E. Frey, P. Fischer, and T. Lied, *Nano Letters* **16**, 906 (2016).
- ¹⁸H. Hrb, J. J. Martin, R. Soheilian, C. Pan, and J. R. Barber, *Advanced Functional Materials* , 3859 (2016).
- ¹⁹G. Grosjean, M. Hubert, G. Lagubeau, and N. Vandewalle, *Physical Review E* **94**, 1 (2016).
- ²⁰J. R. Howse, R. A. L. Jones, A. J. Ryan, T. Gough, R. Vafabakhsh, and R. Golestanian, *Physical Review Letters* **99**, 8 (2007).
- ²¹S. J. Ebbens and J. R. Howse, *Soft Matter* **6**, 726 (2010).
- ²²A. A. Solovev, W. Xi, D. H. Gracias, S. M. Harazim, C. Deneke, S. Sanchez, and O. G. Schmidt, *ACS Nano* **6**, 1751 (2012).
- ²³S. Das, A. Garg, A. I. Campbell, J. R. Howse, A. Sen, D. Velegol, R. Golestanian, and S. J. Ebbens, *Nature communications* **6**, 8999 (2015).
- ²⁴G. Natale, C. Datt, S. G. Hatzikiriakos, and G. J. Elfring, *Physics of Fluids* **29** (2017).
- ²⁵M. Camacho-Lopez, H. Finkelmann, P. Palffy-Muhoray, and M. Shelley, *Nature materials* **3**, 307 (2004).
- ²⁶W. Li, X. Wu, H. Qin, Z. Zhao, and H. Liu, *Advanced Functional Materials* **26**, 3164 (2016).
- ²⁷A. Cebers and I. Javaitis, *Physical Review E - Statistical, Nonlinear, and Soft Matter Physics* **69**, 1 (2004).
- ²⁸R. Dreyfus, J. Baudry, M. L. Roper, M. Fermigier, H. a. Stone, and J. Bibette, *Nature* **437**, 862 (2005).
- ²⁹T. S. Yu, E. Lauga, and A. E. Hosoi, *Physics of Fluids* **18**, 2 (2006).
- ³⁰O. S. Pak, W. Gao, J. Wang, and E. Lauga, *Soft Matter* **7**, 8169 (2011), 1109.1631.
- ³¹W. Gao, D. Kagan, O. S. Pak, C. Clawson, S. Campuzano, E. Chuluun-Erdene, E. Shipton, E. E. Fullerton, L. Zhang, E. Lauga, and J. Wang, *Small* **8**, 460 (2012).
- ³²R. Livanovičs and A. Cebers, *Physical Review E - Statistical, Nonlinear, and Soft Matter Physics* **85**, 5 (2012).
- ³³H. Gadélha, *Regular and Chaotic Dynamics* **18**, 75 (2013).
- ³⁴J. Espinosa-Garcia, E. Lauga, and R. Zenit, *Physics of Fluids* **25** (2013).
- ³⁵I. S. M. Khalil, K. Youakim, A. Sanchez, and S. Misra, *IEEE International Conference on Intelligent Robots and Systems* , 4686 (2014).
- ³⁶I. S. M. Khalil, H. C. Dijkslag, L. Abelmann, and S. Misra, *Applied Physics Letters* **104** (2014).
- ³⁷A. Cebers and K. Erlgis, *Advanced Functional Materials* **26**, 3783 (2016).
- ³⁸F. Box, E. Han, C. R. Tipton, and T. Mullin, *Experiments in Fluids* **58**, 1 (2017).
- ³⁹F. Y. Ogrin, P. G. Petrov, and C. P. Winlove, *Physical Review Letters* **100**, 218102 (2008).
- ⁴⁰A. D. Gilbert, F. Y. Ogrin, P. G. Petrov, and C. P. Winlove, *Quarterly Journal of Mechanics and Applied Mathematics* **64**, 239 (2011).
- ⁴¹A. D. Gilbert, F. Y. Ogrin, P. G. Petrov, and C. P. Winlove, *European Physical Journal E* **34**, 121 (2011).
- ⁴²M. T. Bryan, S. R. Shelley, M. J. Parish, P. G. Petrov, C. P. Winlove, A. D. Gilbert, and F. Y. Ogrin, *Journal of Applied Physics* **121**, 073901 (2017).
- ⁴³J. K. Hamilton, P. G. Petrov, C. P. Winlove, A. D. Gilbert, M. T. Bryan, and F. Y. Ogrin, *Scientific Reports* **7**, 44142 (2017).
- ⁴⁴J. K. Hamilton, M. T. Bryan, A. D. Gilbert, F. Y. Ogrin, and T. O. Myers, *Scientific Reports* **8**, 933 (2018).
- ⁴⁵D. Brown, *Open Source Physics* (Open Source Physics, 2017).
- ⁴⁶C. P. Lowe, *Philosophical Transactions of the Royal Society B: Biological Sciences* **358**, 1543 (2003).
- ⁴⁷J. Happel and H. Brenner, *Low Reynolds number hydrodynamics* (Kluwer, Dordrecht, 1983).
- ⁴⁸L. Landau and E. Lifshitz, *Fluid mechanics* (Butterworth-Heinemann, 1959).

ACCEPTED MANUSCRIPT







Accepted Manuscript

